IAEA nuclear fusion

PAPER

Pedestal confinement and stability in JET-ILW ELMy H-modes

To cite this article: C.F. Maggi *et al* 2015 *Nucl. Fusion* **55** 113031

Nucl. Fusion **55** (2015) 113031 (15pp) doi:10.1088/0029-5515/55/11/113031

Pedestal confinement and stability in JET-ILW ELMy H-modes

C.F. Maggi[1], S. Saarelma[1], F.J. Casson[1], C. Challis[1], E. de la Luna[2], L. Frassinetti[3], C. Giroud[1], E. Joffrin[4], J. Simpson[1], M. Beurskens[1], I. Chapman[1], J. Hobirk[5], M. Leyland[6], P. Lomas[1], C. Lowry[7], I. Nunes[8], F. Rimini[1], A.C.C. Sips[7], H. Urano[9] and JET Contributors[a]

EUROfusion Consortium, JET, Culham Science Centre, Abingdon, OX14 3DB, UK
[1] CCFE, Culham Science Centre, Abingdon OX14 3DB, UK
[2] Asociacion CIEMAT, Madrid, Spain
[3] Association VR, Fusion Plasma Physics, KTH, SE-10044 Stockholm, Sweden
[4] CEA, IRFM, F-13108 Saint-Paul-lez-Durance, France
[5] Max-Planck-Institut für Plasmaphysik, Boltzmannstrasse 2, D-85748, Garching, Germany
[6] York Plasma Institute, Department of Physics, University of York, York YO10 5DD, UK
[7] European Commission, B1049 Brussels, Belgium
[8] Associação IST, Instituto Superior Técnico, Av Rovisco Pais, 1049-001 Lisbon, Portugal
[9] Japan Atomic Energy Agency, 801-1 Muko-yama, Naka, Ibaraki 311-0193, Japan

E-mail: costanza.maggi@ccfe.ac.uk

Received 13 May 2015, revised 18 August 2015
Accepted for publication 14 September 2015
Published 8 October 2015

Abstract

New experiments in 2013–2014 have investigated the physics responsible for the decrease in H-mode pedestal confinement observed in the initial phase of JET-ILW operation (2012 Experimental Campaigns). The effects of plasma triangularity, global beta and neutrals on pedestal confinement and stability have been investigated systematically. The stability of JET-ILW pedestals is analysed in the framework of the peeling–ballooning model and the model assumptions of the pedestal predictive code EPED. Low D neutrals content in the plasma, achieved either by low D_2 gas injection rates or by divertor configurations with optimum pumping, and high beta are necessary conditions for good pedestal (and core) performance. In such conditions the pedestal stability is consistent with the peeling–ballooning paradigm. Moderate to high D_2 gas rates, required for W control and stable H-mode operation with the ILW, lead to increased D neutrals content in the plasma and additional physics in the pedestal models may be required to explain the onset of the ELM instability. The changes in H-mode performance associated with the change in JET wall composition from C to Be/W point to D neutrals and low-Z impurities playing a role in pedestal stability, elements which are not currently included in pedestal models. These aspects need to be addressed in order to progress towards full predictive capability of the pedestal height.

Keywords: pedestal confinement, pedestal stability, H-mode, JET-ILW

(Some figures may appear in colour only in the online journal)

1. Introduction

The first JET experiments with the Be/W ITER-like wall (JET-ILW, MkII-HD divertor geometry, 2011–2012 campaigns) showed a reduction in the low beta (β_N ~ 1.2) ELMy H-mode operation space with good confinement, $H_{98(y,2)}$ ~ 1 (where $H_{98(y,2)} = \tau_E/\tau_{IPB98(y,2)}$): the confinement loss was predominantly found in the pedestal, as the pedestal temperature, T_{PED}, was reduced at all densities, while core pressure profile peaking was largely unchanged [1]. This reduction in normalized confinement is primarily due to the need to operate at

[a] See the appendix of [40].

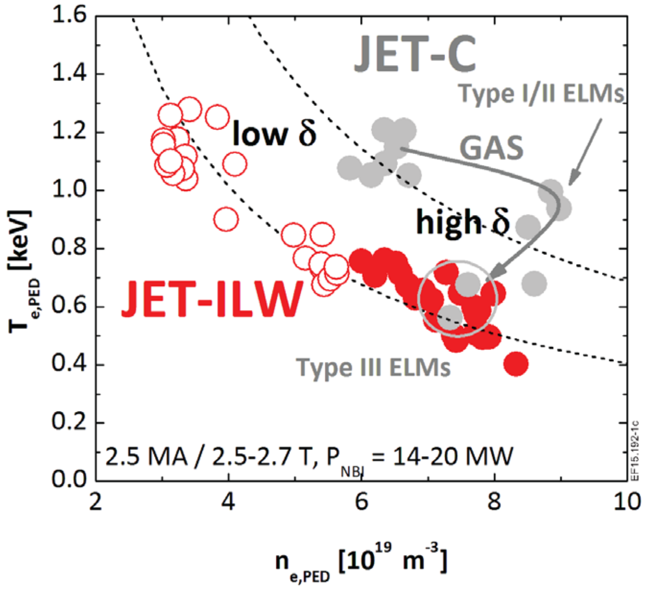

Figure 1. $T_{e,PED}$–$n_{e,PED}$ diagram of JET-ILW type I ELMy H-mode dataset at 2.5 MA/2.5–2.7 T, P_{NBI} = 14–20 MW, β_N ~ 1.5, from the 2013–2014 experiments in red. Open and solid circles are for the low (~0.2) and high (~0.4) δ discharges, respectively, for which similar $p_{e,PED}$ are measured. Comparison with data from a gas scan in JET-C (in grey) at similar input parameters shows that the JET-ILW high δ type I ELMy H-modes occur in conditions typical of type III ELMy H-modes in JET-C. Data are ELM averaged, from the high resolution Thomson scattering diagnostic.

increased D_2 gas rates compared to JET-C in order to avoid large W impurity influxes into the main plasma. In addition to this, higher H-mode performance generally obtained at high triangularity (δ), through improved edge stability with higher plasma shaping, appeared to have been lost: similar pedestal pressure, p_{PED}, was observed at low and high δ in JET-ILW at low β_N [1]. However, an unexpected but positive feature of high δ baseline H-modes was the increase in pedestal pressure with N_2 seeding—used as a tool for divertor heat load mitigation—allowing confinement factors similar to those of JET-C discharges (with the current MkII-HD divertor geometry) to be recovered [2]. In particular, N_2 seeding was found to increase $T_{e,PED}$ in JET-ILW to values approaching those of JET-C at similar $n_{e,PED}/n_{GW}$, while core confinement was not improved, as pressure peaking remained unaffected by N_2 seeding. Also in the case of high beta H-modes the pedestal pressure appeared to be lower in JET-ILW, but the global normalized energy confinement remained comparable to that in JET-C as the reduction in pedestal confinement was compensated by increased core profile peaking [3]. When assessing the edge stability of JET ELMy H-mode plasmas, JET-C pedestals are typically found to be close to the peeling–ballooning (P–B) limit before a type I ELM crash, while the 2011/12 JET-ILW H-modes at low beta (<1.5) and high D_2 gas injection rates (without N_2 seeding) were found deep in the stable region [4], primarily due to the lower $T_{e,PED}$ compared to JET-C.

In order to address the physics responsible for the decrease in pedestal confinement in the initial phase of the JET-ILW experimental campaigns, new experiments were carried out during the 2013–2014 campaigns. The new investigations reported in this paper focus on the following aspects: (i) the effect of plasma triangularity; (ii) the effect of beta and (iii) the effect of neutrals on JET-ILW pedestal confinement and stability, reporting on the progress achieved since the 2012 IAEA Fusion Energy Conference. In general, the experiments indicate that while the pedestal energy confinement has been affected by the changes in wall material from JET-C to JET-ILW, the pedestal density has remained largely unaffected. The stability of JET-ILW pedestals is investigated in the framework of the P–B model [5, 6] and the pedestal predictive model EPED [7, 8], currently the leading model for predictions of the pedestal height in ITER and DEMO. The constraint of preventing core W accumulation on longer confinement timescales requires the use of D_2 gas puffing, leading to increased neutral pressure in the main chamber and reduced pedestal temperature. The strong reduction in pedestal temperature at high gas rates pushes the pedestal to the high-n ballooning corner of the edge stability diagram. In these conditions additional physics in the pedestal models may be required to explain the onset of the ELM instability.

The paper is organized as follows: the effect of plasma triangularity on pedestal confinement and stability is discussed in section 2, the effect of beta is presented in section 3, section 4 addresses the effect of neutrals and in section 5 conclusions are drawn.

2. Effect of plasma triangularity

In JET-ILW low β_N H-modes, relatively high levels of D_2 gas injection are required for W control. In these plasmas the beneficial effect of plasma shaping on pedestal confinement, commonly found in many tokamaks both experimentally and numerically (see e.g. [9]), is not observed, since low and high δ H-modes exhibit similar pedestal pressures. Typically, $T_{e,PED}$ is lower than in JET-C at similar values of $n_{e,PED}/n_{GW}$ [1]. This is illustrated in the edge diagram of figure 1 for a dataset of ELMy H-modes at 2.5 MA/2.5–2.7 T, with NBI input power ranging from 14 to 20 MW, comparing the JET-ILW type I ELMy discharges from the recent 2013–14 experiments (in red) with data from a D_2 gas scan in JET-C (in grey) at similar input parameters [9]. The data are ELM averaged from the high resolution Thomson scattering diagnostic (HRTS). The JET-C high δ dataset could be fuelled up to the Greenwald density while maintaining good confinement ($H_{98(y,2)}$ ~1). This was connected with a transition from pure type I ELMs to mixed type I/II ELMs at the highest densities, see figure 1 and [3, 11–13]. The pedestals of the JET-ILW high δ H-modes (full red circles) are found on the same isobar as the pedestals of low δ H-modes, which in 2013–14 could be optimized towards stable operation at lower densities than those achieved during the initial ELMy H-mode phase with ILW (see section 4.3). Moreover, the high $n_{e,PED}$ and low $T_{e,PED}$ values of these JET-ILW high δ type I ELMy H-modes are similar to those of type III ELMy H-modes in JET-C, obtained at the highest gas rates of the fuelling scan [2]. A comparison of density ramp experiments in JET-C and JET-ILW at similar I_P/B_T has also revealed a reduction in pedestal temperature

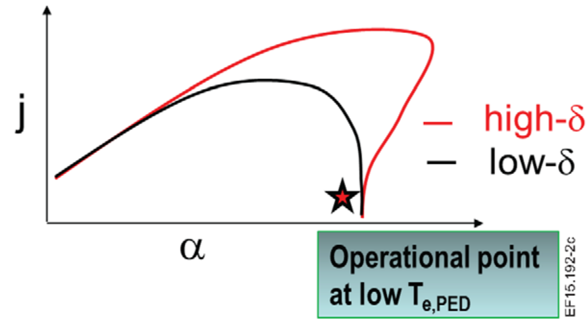

Figure 2. Cartoon of a j–α stability diagram, illustrating an operational point at low $T_{e,PED}$–high ν^*_{PED} and low bootstrap current (red star) and the stability boundaries for low (black) and high (red) plasma shape. Increasing δ at high $\nu*$ does not raise the pedestal height. This is the likely situation for JET-ILW low beta/high collisionality type I ELMy H-modes, where similar pedestal pressures are found at low and high δ.

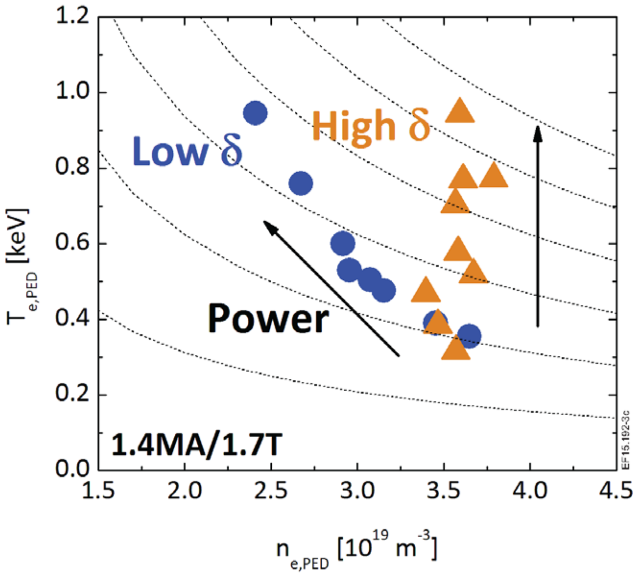

Figure 3. $T_{e,PED} - n_{e,PED}$ diagram for the 1.4 MA/1.7 T JET-ILW power scans at low gas injection ($\Gamma_D \sim 3\times 10^{21}$ e s^{-1}) at low (orange) and high (blue) δ, for (V/H) divertor configuration in MkII-HD divertor geometry. High and low δ plasmas have similar pedestal pressure at low power/beta. High δ plasmas (orange triangles) have higher electron pressure than the low δ (blue circles) H-modes at high power/beta. Data are from composite HRTS profiles in the last 30% of the ELM cycle.

at which the type I ELM regime is accessed in JET-ILW [3], possibly indicating a lower type/type III ELM threshold than in JET-C. In addition, both the edge temperature and the loss power at which the L–H transition occurs are reduced in JET-ILW in the high density branch [14]. However, all this does not translate to a confinement benefit for type I ELMy H-modes in JET-ILW.

The physics mechanism resulting in lower $T_{e,PED}$ in JET-ILW H-modes is not yet understood and is under investigation. However, its implication on the pedestal stability can be understood within the P–B paradigm, as illustrated graphically in the j–α diagram of figure 2 (with j the edge current and α the dimensionless pressure gradient, $\alpha = (2\partial_\psi V)/(2\pi)^2(V/2\pi^2R)^{1/2}\mu_0 p'$, where V is the volume enclosed by the flux surface, R is the major radius and p' is the pressure derivative with respect to the poloidal flux ψ). The operational point at low $T_{e,PED}$ (red star in the diagram) and thus high pedestal collisionality, ν^*_{PED}, and low bootstrap current, j_{BS}, is located in the ballooning region of the stability diagram. In these conditions the P–B model predicts little or no improvement in pedestal pressure with increasing δ due to the strong reduction in the edge bootstrap current [9]. A similar stability boundary is expected both at low and high δ (black and red curves, respectively, in the diagram of figure 2) as indeed is observed in the low β_N ($\beta_N < 1.5$), low T_{PED}, JET-ILW H-mode dataset of figure 1. In such conditions a mere increase in triangularity does not recover the pedestal height.

On the other hand, H-mode operation at high β_N and low D_2 gas injection rates has not led to energy confinement degradation after the JET wall changeover from CFC to Be/W plasma facing components, both at low and high triangularity, as reported in [15]. Therefore, in order to separate the effect of beta from that of gas injection on pedestal confinement and stability, new power and gas scan experiments were carried out in 2013–2014. In the next section we first address the effect of beta on the confinement and stability of JET-ILW H-mode pedestals.

3. Effect of beta: power scans at low D_2 gas injection

New power scans were carried out in the 2013–2014 campaigns with low D_2 gas injection rates, $\Gamma_D \sim 2.8\times 10^{21}$ e s^{-1}, at $I_P = 1.4$ MA, $B_T = 1.7$ T, both at low ($\delta \sim 0.2$) and high ($\delta \sim 0.4$) δ shapes [15]. As the input power (beta) is increased in subsequent discharges, the pedestal top pressure increases rapidly both at low and high δ, as shown in figure 3, contributing to the weak power degradation of global energy confinement observed in JET-ILW at high beta [15]. Other factors that contribute to the good confinement observed at high beta include density peaking at low collisionality, longer fast ions slowing down time resulting in larger fast ion pressure and increased core turbulence suppression due to electromagnetic effects, as analysed in detail in [15]. Here we concentrate on the pedestal effects. The data shown in figure 3 refer to the last 30% of the type I ELM cycle and are obtained from *mtanh* [16] fits of composite HRTS profiles over the steady time window selected for the analysis. At high δ the increase in pedestal pressure is somewhat stronger than at low δ (see figure 3), as $T_{e,PED}$ increases with power/beta at constant $n_{e,PED}$. At low δ the increase in $T_{e,PED}$ is accompanied by some reduction in $n_{e,PED}$, however a concomitant increase in core density peaking results in the observed weak power degradation of the total energy confinement found also at low δ [15]. The pedestal pressure of high δ, high β_N H-modes, where high T_{PED} and thus low ν^*_{PED} values are achieved, is about 30% higher than at low δ. Conversely, at low beta (higher collisionality), similar pedestal pressures are observed, a result

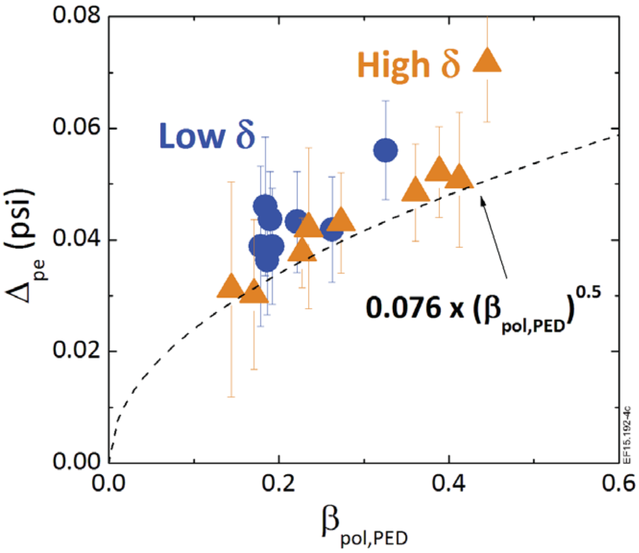

Figure 4. Electron pedestal pressure width in psi space versus pedestal poloidal beta for the low and high δ power scans of figure 3 compared to the KBM-based pedestal width scaling of $0.076 \times \sqrt{\beta_{\mathrm{pol,PED}}}$ in the EPED model.

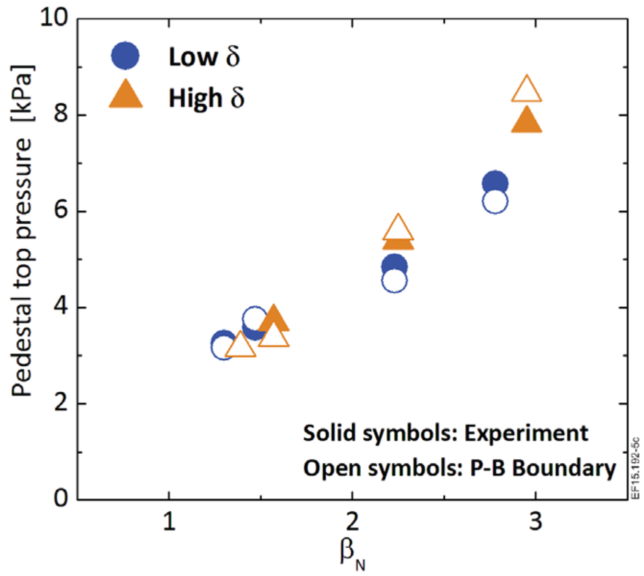

Figure 5. Comparison of total pedestal top pressure from experiment (solid symbols) and P–B boundary for type I ELM crash, as calculated by HELENA/ELITE (open symbols), versus β_{N} for the low and high δ power scans at low gas injection of figure 3.

which is consistent with the findings presented in section 2 and shown in figure 1 for the dataset at 2.5 MA/2.7 T.

As the input power is increased in the experiment, the pedestal top poloidal beta, $\beta_{\mathrm{pol,PED}}$, increases while the collisionality $\nu^*_{\mathrm{e,PED}}$ decreases in a correlated fashion, as typically found in power scan experiments. In order to verify experimentally for JET-ILW the scaling of the pedestal width with sqrt($\beta_{\mathrm{pol,PED}}$), which is assumed in the EPED model [7, 8] the variation of the pedestal pressure width would need to be investigated in a dimensionless β_{pol} scan, at constant ν *, ρ* and q_{95}. This is work in progress. However, analysis of the electron pedestal structure of the low and high δ power scans at low D_2 injection can already provide useful information regarding the scaling of the pedestal width in JET-ILW. Figure 4 indicates that the pedestal pressure width increases with pedestal poloidal beta in ψ space, especially in the dataset at high δ, and that the trend appears to be consistent with an increase proportional to sqrt($\beta_{\mathrm{pol,PED}}$). For consistency with the formulation in EPED, the pedestal pressure width is derived here as the mean of the T_{e} and n_{e} widths, evaluated separately in the last 30% of the ELM cycle, using the method described in [17]. We note that in these power scans the pedestal width increases in ψ space. Within the experimental uncertainty no clear increase has been observed in real space (at the outboard midplane). Therefore the pedestal broadening in ψ space can be associated with the increase in Shafranov shift, which compresses the flux surfaces at the low field side. The pedestal pressure gradient is also found to increase with beta, thus the increase in $p_{\mathrm{e,PED}}$ with power is due to an increase in both pedestal width and gradient with beta.

The edge stability of these pedestals was investigated with the ideal MHD stability code ELITE [5, 6], with input the measured pre-ELM pressure profiles and using the Sauter model [18, 19] to calculate the contribution of the bootstrap current, j_{BS}, to the total edge current. $T_{\mathrm{i}} = T_{\mathrm{e}}$ is assumed (consistent with charge exchange measurements) and the line averaged Z_{eff} from visible Bremsstrahlung is used in the calculation of the main ion density (with Be the main intrinsic impurity) and j_{BS}. The analysis indicates that the pressure gradient before the type I ELM crash is in good agreement with the limit set by finite-n peeling–ballooning instabilities, both at low and high δ, across the entire power scan at low gas injection, which results in beta values ranging from $\beta_{\mathrm{N}} \sim 1.5$ to $\beta_{\mathrm{N}} \sim 3$ [18, 19]. This is illustrated in figure 5, where the experimental total pedestal top pressure is compared for each point of the power/β_{N} scan to the corresponding predicted pedestal top pressure at the P–B boundary, showing good agreement. The higher pedestal pressure obtained at high beta with the high δ shape is also consistent with the model predictions. In particular, increasing core pressure stabilizes the ballooning modes due to the increased Shafranov shift, thereby raising the P–B boundary (see also [18, 19] for further details). In summary, we find that the pedestal stability of JET-ILW H-modes at low D_2 gas injection is consistent with the P–B model, both at low and high δ and both at low and high β_{N}.

We note, however, that the minimal D_2 gas injection rates used for these power scans, although entirely suitable for comparative confinement studies of JET-ILW and JET-C H-modes [15], are not always compatible with stable ELMy H-mode plasma conditions over longer time scales, which require integration of the constraints imposed by operation with the W divertor [21]. After achieving the conditions plotted in figure 3, the discharges at low D_2 gas rate typically display a continuous increase in core radiated power over longer time scales (2–10 $\times$ τ_{E}), a sign of increasing core W concentration, although the plasmas remain in H-mode during the heating and I_{P} flat top phase and the discharges do not end with radiative collapse. Higher D_2 gas injection levels are typically needed to maintain low enough divertor target temperatures to reduce W sputtering and therefore control W influxes through

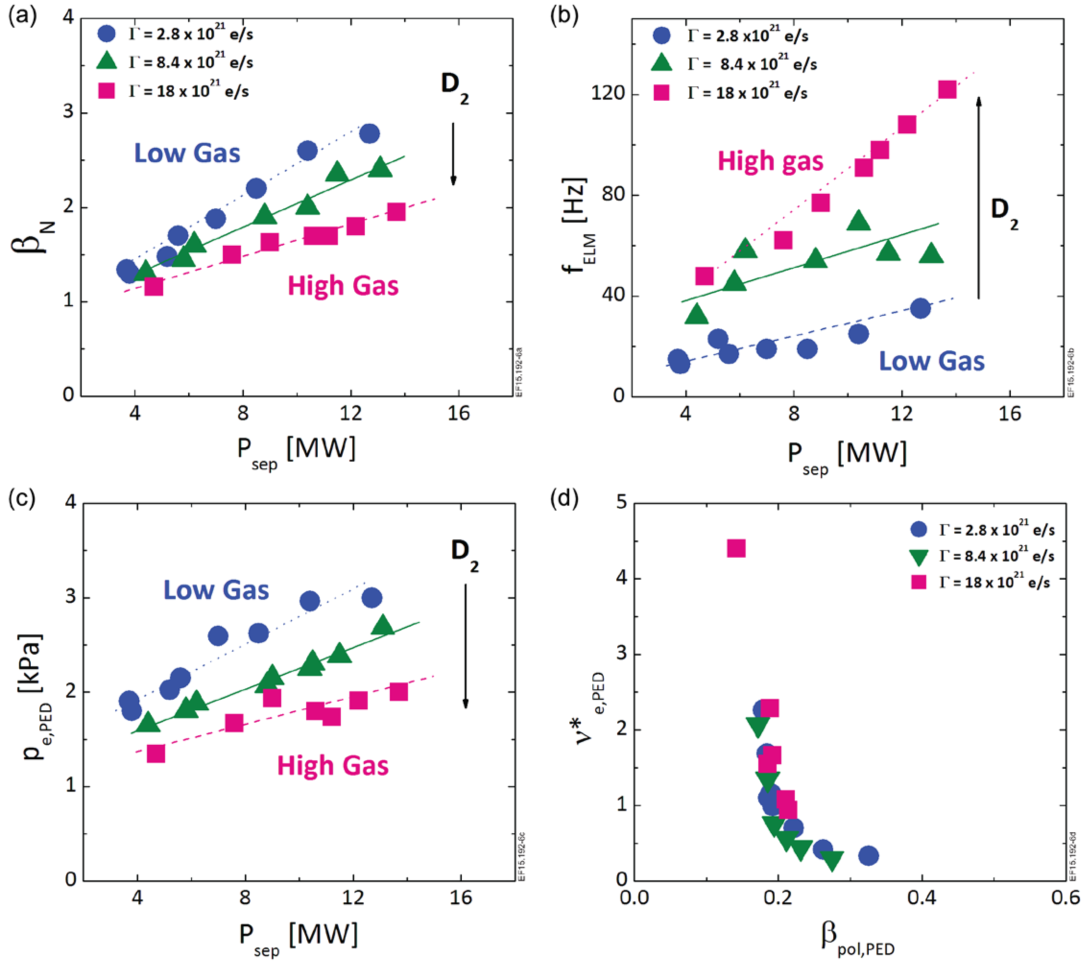

Figure 6. Total normalized beta (*a*), ELM frequency (*b*), and ELM-averaged electron pedestal pressure (*c*) versus $P_{sep} = P_{heat} - dW/dt - P_{rad,bulk}$ for the three power scans at 1.7 T/1.4 MA at low δ, with increasing levels of D_2 gas injection. All discharges are in the type I ELMy regime. (*d*) Pedestal top collisionality and poloidal beta ranges obtained in the same experiments (pre-ELM values, from HRTS only).

the pedestal into the core plasma. In addition, increasing D_2 gas injection increases the ELM frequency, thus facilitating W flushing by ELMs. The combination of these two effects allows stable ELMy H-mode operation with the ITER-like wall. In this work a stable discharge is defined as having main plasma parameters constant within 10% of their ELM-averaged values over at least $4 \times \tau_E$, typically throughout the entire I_P flat-top and main heating phase (~$10 \times \tau_E$ or longer).

The power scan at low δ was thus repeated at higher D_2 gas injection rates, typical of JET-ILW steady H-mode conditions, to provide a connection with the ELMy H-mode operational space at higher I_P/B_T and to enable a systematic study of the separate effects of beta and gas injection (or neutral content in the plasma) on pedestal confinement and stability. These experiments are discussed in the next section.

4. Effect of neutrals

4.1. Power and D_2 gas scans

The low δ power scan at low gas injection was repeated at two, higher D_2 gas injection rates, roughly doubling the average gas rate from one power scan to the next, from 2.8 to 8.4 to 18×10^{21} e s^{-1}. The maximum achieved β_N— at similar P_{sep} ~ 13 MW (where P_{sep} is the net power across the separatrix, $P_{sep} = P_{heat} - dW/dt - P_{rad,bulk}$)—decreases with increasing D_2 gas rate, from 2.75 down to 1.95, as shown in figure 6(*a*). Nonetheless, all discharges are found to be in the type I ELMy H-mode regime, according to the usual definition of ELM frequency, f_{ELM}, increasing with P_{sep} [22] as shown in figure 6(*b*). Figure 6(*b*) also shows that the three power scans belong to three separate branches with respect to beta and ELM frequency, both in terms of their absolute values and in terms of their rate of increase with P_{sep}. In particular, in the plasmas with low D_2 injection rate the ELM frequency remains low and increases much more weakly with power than in the plasmas with highest D_2 rate.

Pedestal top temperatures and densities are derived from *mtanh* fits of ELM-averaged composite profiles of HRTS and ECE data for T_e and HRTS and Li-beam data for n_e for the three power scans. Figure 6(*c*) shows the variation of $p_{e,PED}$ versus P_{sep} as the gas injection rate is increased in the three power scans. At all power levels the pedestal pressure is reduced with high gas injection compared to cases with low gas injection.

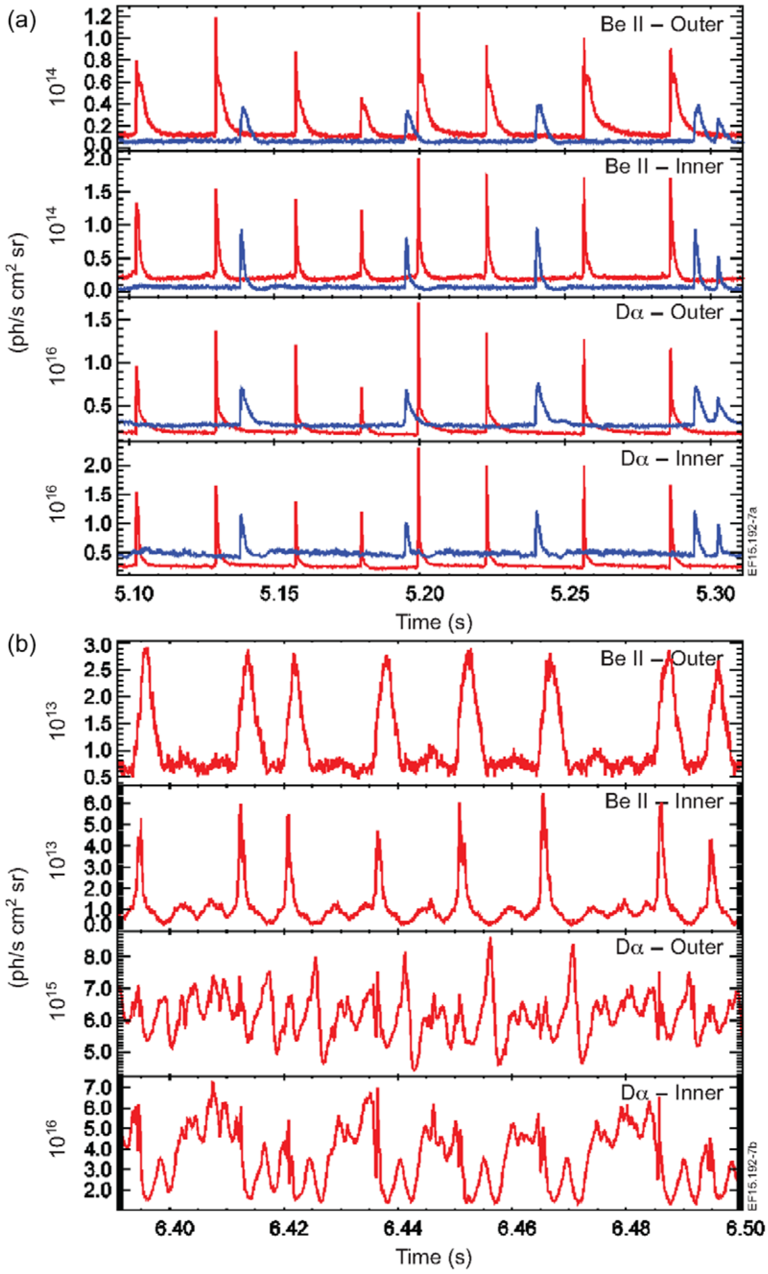

Figure 7. Outer and inner divertor Be II (527 nm) photon fluxes (top two panels), used as ELM markers in JET-ILW, and evolution of D_α photon fluxes during the corresponding ELM cycles (bottom two panels). (*a*) ELM signatures from the power scan at low gas injection, at lowest (blue, #84793) and highest (red, # 84794) β_N in the scan. (*b*) ELM signatures and D_α fluxes for discharge #87344 with high gas injection ($\beta_N = 1.63$, $f_{ELM} = 77$ Hz). All three H-modes are type I ELMy, as shown in figure 6(*b*).

On average $n_{e,PED}$ is largely insensitive to the increase in D_2 gas rate and also decreases weakly with increasing input power. On the other hand, $T_{e,PED}$ is mostly affected by the increase in gas injection, on average decreasing by a factor of two as the D_2 gas rate increases from lowest to highest and it increases with power for a given D_2 gas rate. Therefore the strong variation in pedestal collisionality obtained in the power and gas scan experiments at low δ (figure 6(*d*)) is mainly driven by the variation in pedestal top temperature, while the variations in $n_{e,PED}$ and Z_{eff} contribute more weakly to it. As expected, the variations in $\nu^*_{e,PED}$ and $\beta_{pol,PED}$ are correlated in these experiments. Figure 7 shows that also the inter-ELM evolution of these plasmas are qualitatively very different between the power scan at lowest and highest D_2 rate, as illustrated by the time traces of the inner and outer divertor Be II and D_α photon fluxes.

Analysis of the pre-ELM pedestal structure (namely in the last 30% of the ELM cycle) indicates that the electron pressure width in ψ space widens with increasing D_2 gas rate, as shown in figures 8(*a*) and (*b*). To try and reduce scatter in the data, Δ_{pe} is normalized to $(\beta_{pol,PED})^{0.5}$, under the assumption that the EPED width scaling holds for JET-ILW pedestals, as could be indicated by the data of figure 4. It is interesting to note that with this normalization also the pedestal pressure

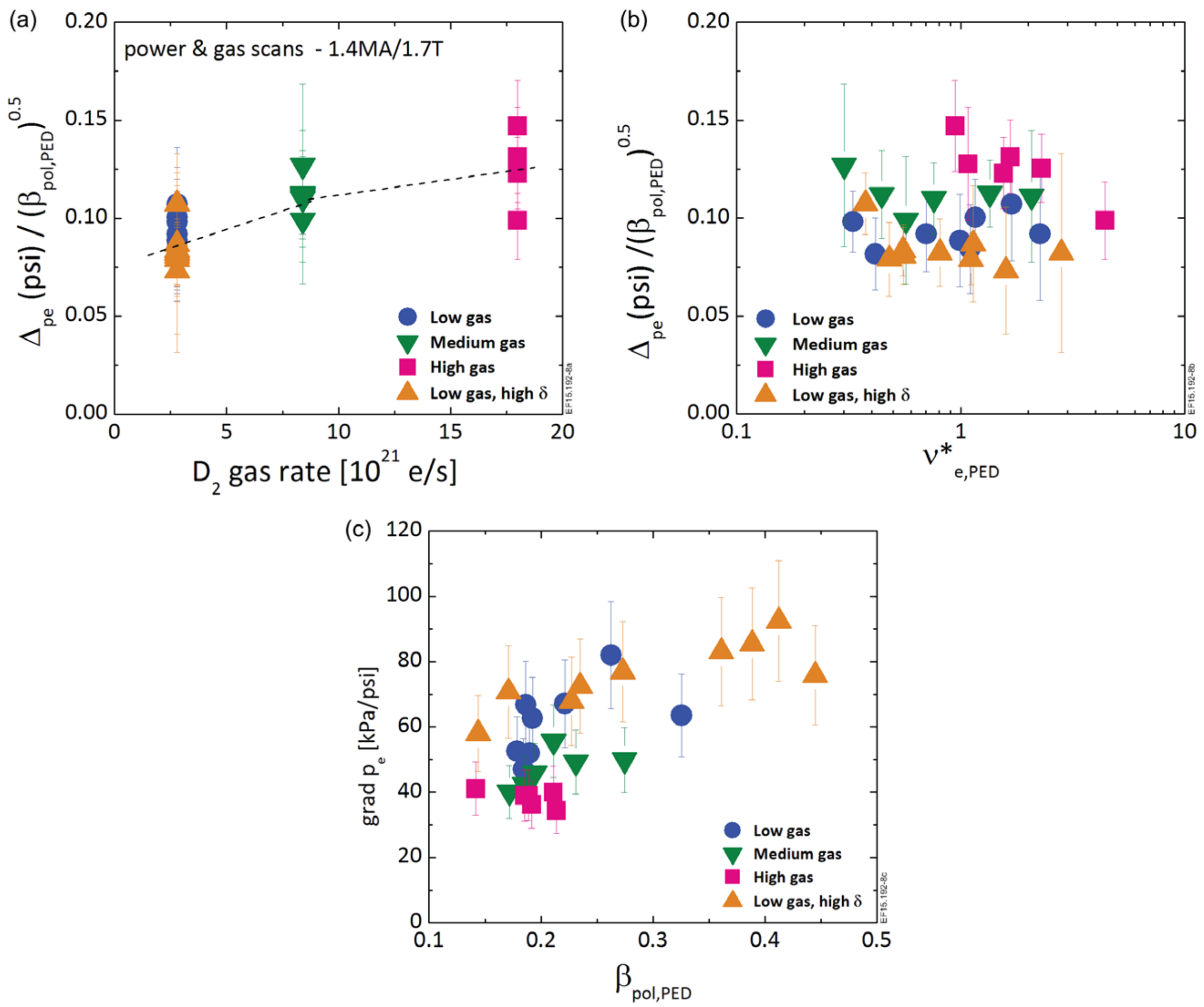

Figure 8. (*a*) Pedestal electron pressure width in ψ space, normalized to sqrt($\beta_{pol,PED}$) versus D_2 gas rate for the power and gas scans at low δ and for the low gas power scan at high δ; (*b*) normalized pedestal electron pressure width versus pedestal top collisionality; (*c*) electron pressure gradient versus $\beta_{pol,PED}$. All data are from the last 30% of the ELM cycle.

widths of the high δ power scans at low gas rate fall in line with the trend of Δ_{pe} increasing with D_2 gas level. On the other hand, $\Delta_{pe}/(\beta_{pol,PED})^{0.5}$ shows no appreciable variation with $\nu^*_{e,PED}$. The pressure gradient increases with $\beta_{pol,PED}$ at low D_2 gas rate, as discussed in section 3, whereas at medium to high gas rate it remains constant, as shown in figure 8(c). Therefore the weaker increase in $p_{e,PED}$ at medium/high D_2 gas rates is due to broadening of the pedestal width at constant gradient. It is to note that in this analysis the fractional interval of the ELM cycle is the same (the last 30% before the ELM crash) at all three levels of gas rates, whereas the ELM dynamics changes significantly with increasing D_2 gas rate, as shown in figures 7(*a*) and (*b*). Therefore it cannot be excluded that the choice of fractional interval of the ELM cycle plays a role when investigating the pedestal structure of a D_2 gas scan. This aspect is currently being investigated and will be reported in a future work.

The evolution of the pedestal structure in the power and gas scans, discussed above, exhibits similarities with the measurements obtained in D_2 gas scans at constant input power in 2.5 MA/2.7 T high δ ELMy H-modes, analyzed in detail in [23]. In those experiments, with increasing D_2 gas rate the pressure gradient decreases and the width increases at constant $\beta_{pol,PED}$ [23]. In particular, the increase in D_2 gas rate at constant input power results in the increase in $\nu^*_{e,PED}$ at constant $\beta_{pol,PED}$. These observations challenge the EPED model assumptions, as the pedestal widens at constant $\beta_{pol,PED}$ but with increasing $\nu^*_{e,PED}$ (D_2 gas rate), thus deviating from the KBM-based dependence of the pedestal width with sqrt($\beta_{pol,PED}$).

These observations may indicate an additional dependence of the pedestal pressure width on other parameters than only $\beta_{pol,PED}$, either directly or indirectly connected with D neutral penetration in the pedestal region.

4.2. Edge stability analysis

In order to assess the effect of increased neutral content in the plasma on the pedestal stability, ELITE numerical runs were carried out at the lowest and highest β_N range of the power scans at the three D_2 gas injection rates. The results

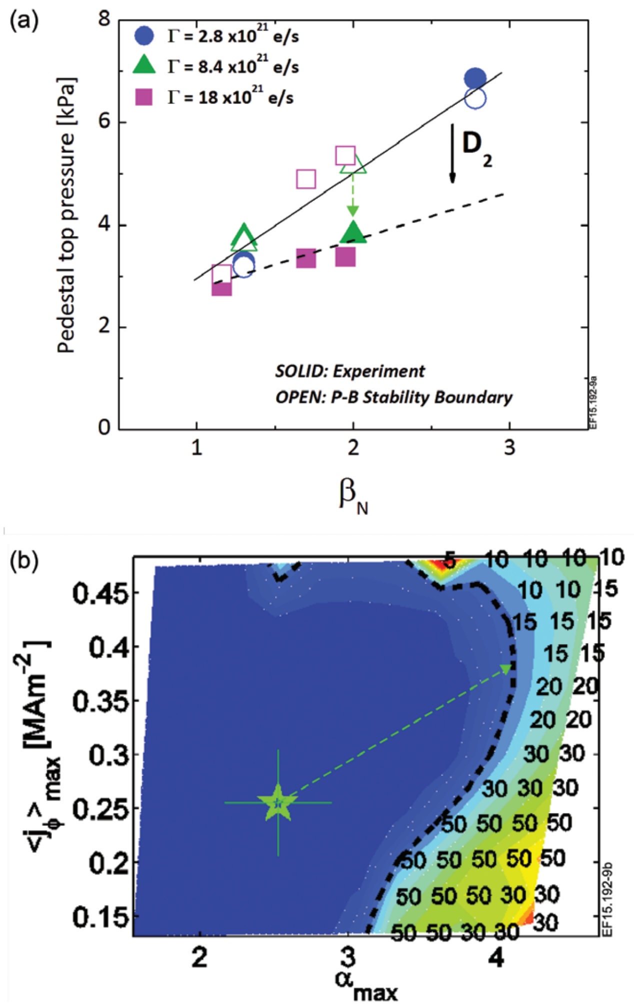

Figure 9. (*a*) Comparison of P–B stability limit (open symbols) and experimental point (solid symbols) at low (blue), intermediate (green) and high (magenta) D_2 gas rates as a function of β_N for a subset of discharges of the low δ power and gas scans of figure 5. The distance of the operational point to the P–B boundary is indicated by the green arrow, calculated self-consistently with ELITE at pedestal width fixed to the experimental value and increasing $T_{e,PED}$. Figure 9(*b*) exemplifies in 2D in the corresponding *j*–α diagram. (*b*) *j*–α stability diagram illustrating the distance of the operational point (green star) from the P–B boundary—represented by the length of the green arrow—as calculated with HELENA/ELITE at pedestal width fixed to the experimental value and increasing $T_{e,PED}$, with $n_{max} = 50$ and $\gamma > 0.0\,3\times\,\omega_A$ as stability criterion. The case is for pulse #87341, $P_{sep} = 10.4$ MW ($\beta_N = 2$), $\Gamma_D = 8.4\times\,10^{21}$ e s^{-1}. In (a), the operational point corresponds to the green solid triangle and its distance from the stability boundary (open green triangle) is indicated by the green, broken arrow.

are summarized in figure 9(*a*). Here the same representation of figure 5 is used, namely solid symbols for the experimental total pedestal top pressure and open symbols for the calculated pressure at the P–B stability boundary. In this representation, the distance of the operational point to the P–B boundary is given by the length of the green arrow for the data point at $\beta_N \sim 2$ (JET pulse #87341, gas rate $= 8.4\,\times\,10^{21}$ e s^{-1}). Figure 9(*b*) exemplifies the same case in the j_{edge}–α_{max} diagram, where the operational point is represented by the green star and the distance to the P–B boundary—illustrated by the green dashed arrow—is calculated self-consistently at pedestal width fixed to the experimental value and increasing $T_{e,PED}$. The stability calculations were carried out for toroidal mode numbers up to $n = 50$ (see e.g. figure 9(*b*)) and using $\gamma > 0.0\,3\times\,\omega_A$ as stability criterion (with γ the growth rate and ω_A the Alfvén frequency), as previously done for stability analysis of JET-C pedestals [24]. Accordingly, at low gas rate (blue circles in figure 9(*a*)) the pedestals are found near the P–B stability boundary before the ELM crash, both at high and low beta as discussed in section 3 (see figure 5). In contrast, at intermediate and high D_2 gas rates (green and magenta symbols in figure 9(*a*)) the type I ELMy H-mode pedestals are found to be deeply stable to intermediate-*n* P–B instabilities at higher β_N. Thus, the weaker increase in pedestal pressure with power observed at high D_2 gas rates does not appear to be consistent with the P–B model, at least in the ELITE calculations run with the assumptions described above. As these type I ELMy pedestals are characterized by low edge current and high collisionality, and thus populate the ballooning region of the stability diagram, possible sources of discrepancy between experiment and P–B model could be connected with the model used for the calculation of the bootstrap current and/or with larger uncertainties in the definition of the stability boundary for pure high-*n* ballooning modes. In the following sections we address these issues separately. Given that the operating points of the pedestals with strong gas puffing have very little coupling of peeling drive with ballooning drive, it is perhaps not surprising that the EPED model assumptions do not apply to this corner of *j*–α space. It may also be that the ELMs we observe in conditions of high neutral content, despite being of type I according to the empirical definition of increasing ELM frequency with power, are of resistive nature—e.g. more similar to type III ELMs—and therefore not described by the P–B paradigm.

4.2.1. Impact of bootstrap current models on the edge stability results. One possible source for the discrepancy between the results of the ELITE stability analysis and the experimental data may be connected with the calculation of the edge bootstrap current in conditions of high collisionality, achieved in our case at high D_2 gas injection. A recent comparison between simulation results with the drift kinetic code NEO [25, 26] and the Sauter model [18, 19] for low and high collisionality DIII-D discharges has shown the Sauter model to overestimate j_{BS} at high collisionality and to underestimate it at low collisionality [27]. This work thus motivated comparison of the two bootstrap current models for the experimental conditions of the JET-ILW pedestals of the power and gas scans. For the NEO runs we have assumed equal electron and ion temperatures, constant line averaged Z_{eff}, a single impurity species (=Be) and local, no orbit effects. Starting from the experimental profiles, the sensitivity of the two j_{BS} models to variations in collisionality and in Z_{eff} have been investigated by means of temperature and Z_{eff} scans, respectively. It is found that in order to test the accuracy of the Sauter model a good figure of merit is the value of $\nu*$ at the peak of the pedestal current. The key results of the analysis can be summarized

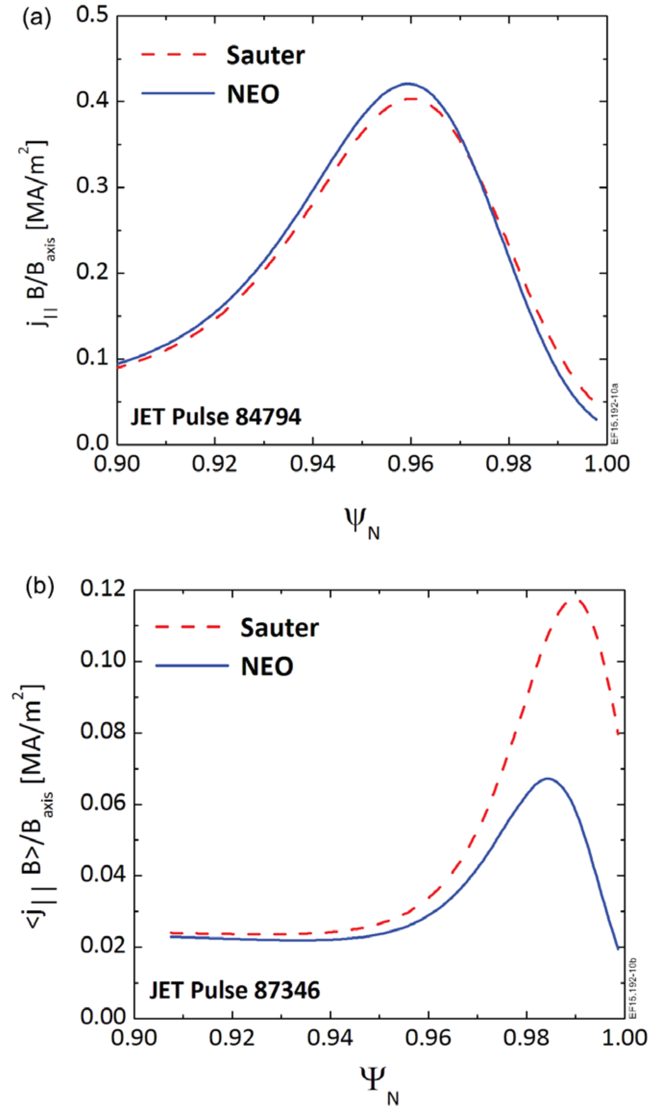

Figure 10. Comparison of edge bootstrap current profiles calculated with Sauter's formula [18, 19] and with NEO [25, 26] for the JET pedestals (*a*) at low gas, high power (#84794) and (*b*) at high gas, low power (#87346), this being the case with the lowest j_{BS} of the power and gas scans. The two calculations agree well at low collisionality (case (*a*)), except near the separatrix, whereas at high collisionality (case (*b*)) the Sauter calculation overerstimates that from NEO by almost 100%.

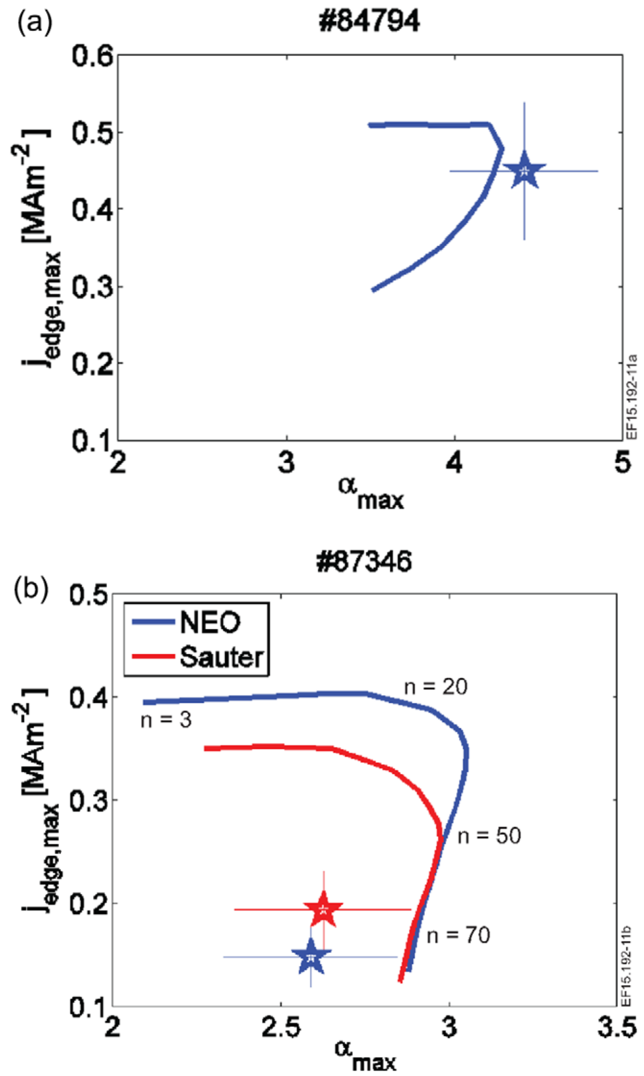

Figure 11. Comparison of the effect of j_{BS} model, Sauter (red) and NEO (blue), on the pedestal stability analysis for: (*a*) low gas, high power case #84794 (=low collisionality) where the two models are not distinguishable in the edge stability analysis and (*b*) high gas, low power pedestal #87346 (high collisionality). The ELITE calculations were run with $n_{max} = 70$ and $\gamma > 0.03\omega_A$.

as follows: (i) at low collisionality ($\nu^* < 1$) and $Z_{eff} \sim 1$, the Sauter and NEO models agree very well; (ii) at high collisionality ($\nu^* > 1$) and $Z_{eff} \sim 1$, the Sauter model overestimates j_{BS}, relative to NEO, in agreement with the results of [27]; (iii) for $Z_{eff} \gg 1$ an additional, competing effect is found, which causes the Sauter model to underestimate j_{BS} relative NEO: at $\nu^* > 1$ this effect can compensate the overestimate of Sauter wrt NEO, leading to very similar j_{BS} values in the two cases, while at very low collisionality (so far, usually found radially inwards of the peak of j_{BS}) it will always cause the Sauter model to underestimate j_{BS}. Figure 10 shows the two extreme examples of this case study: figure 10(*a*) compares the edge bootstrap current profiles calculated with Sauter's formula and with NEO for a JET-ILW pedestal at low collisionality (low gas, high power pulse #84794) while figure 10(*b*) shows the comparison for the pedestal at highest collisonality and lowest j_{BS} in the scan (high gas, low power shot #87346). The two calculations agree well at low collisionality, except near the separatrix, whereas at high collisionality the Sauter calculation overerstimates that from NEO by almost 100%. Figure 10(*b*) shows that the difference in shape between the two j_{BS} models is linked to collisionality, which increases strongly as one approaches the separatrix region. In this region j_{BS} from NEO is strongly reduced compared to j_{BS} from Sauter.

Comparative ELITE runs with j_{BS} calculated according to Sauter's formula (in red) and NEO (in blue) are shown in figure 11 for the pedestal at low (low gas/high power, #84794) and highest collisionality (high gas/low power, #87346) of the power and gas scans. The ELITE calculations were run with $n_{max} = 70$ and $\gamma > 0.03\omega_A$ was used to define the stability criterion. At low collisionality (figure 11(*a*)) the two bootstrap current models give identical results (not distinguishable in the figure). On the other hand, in the high collisionality case the choice of j_{BS} model influences the edge stability: the NEO calculations drive the operational point to lower maximum edge current and also modify the peeling boundary (figure 11(*b*)). In particular, the reduction in j_{BS} near the separatrix obtained with NEO reduces the growth rate of current driven low-n peeling modes and thus results in an expansion of the peeling boundary (blue stability boundary in figure 11(*b*)) compared to the case with j_{BS} from Sauter's model (red stability boundary in figure 11(*b*)). However, in both cases the operational point is close to the ballooning boundary within ~15% and the overall difference between the two stability analyses is certainly not larger than the uncertainties in the experimentally measured pressure gradient and definitely smaller than other uncertainties associated with the stability analysis procedure, as discussed in the following sections. The peeling boundary changes more with the choice of the bootstrap current model. This is due to changes in the shape of the current profile, as shown in figure 10(*b*). Compared to NEO, Sauter's formula gives higher current at the foot of the pedestal near the separatrix, which is destabilising for the peeling modes, therefore reducing the peeling boundary [28]. However, this modification does not affect the result of the stability analysis of the cold, high ν* pedestal of pulse #87346, which is limited by high-n ballooning modes.

Of all pedestals of the JET-ILW low I_P, power and gas scans, the one of pulse #87346 is that where we find the largest reduction in edge bootstrap current with NEO compared to the Sauter formula. From the sensitivity study described above we conclude that in conditions of high pedestal collisionality the NEO model for j_{BS} should be adopted. However, this more accurate j_{BS} model does not fully account for the discrepancy between the weaker increase in p_{PED} with beta at high D_2 gas rates observed experimentally and the P–B model predictions, as shown in figure 9.

4.2.2. Impact of stability criteria on the shape of the stability boundary. In the stability diagrams of figures 11(*a*) and (*b*), $\gamma > 0.03\omega_A$ defines the stability criterion (as e.g. in the diagram of figure 9(*b*)). However, the choice of stability criterion is somewhat arbitrary and $\gamma > c\omega^*_{max}$ is also often used in the literature [9], with c a constant <1. As ω^*_{max} is proportional to the pressure gradient and varies strongly in the pedestal, which value to use for c is also a matter of debate. For this investigation we select $c = 0.25$. The choice of stability criterion can have a larger impact on the ELITE calculations of the pedestals under study, as shown in figures 12(*a*) and (*b*). In the low collisionality case (#84794, figure 12(*a*)), where the Sauter and NEO j_{BS} calculations are in agreement, no difference is found in the operational point (red star coinciding with blue star), but the ballooning boundary expands when $\gamma > 0.25\omega^*_{max}$ is chosen (blue dashed line) since the diamagnetic stabilisation is proportional to the toroidal mode number n. From the point of view of the comparison of the numerical results with the experimental point, though, this hardly matters, as the operational point lies close (within experimental uncertainties) to the stability boundary for intermediate n P–B modes, where very little difference is found in the two

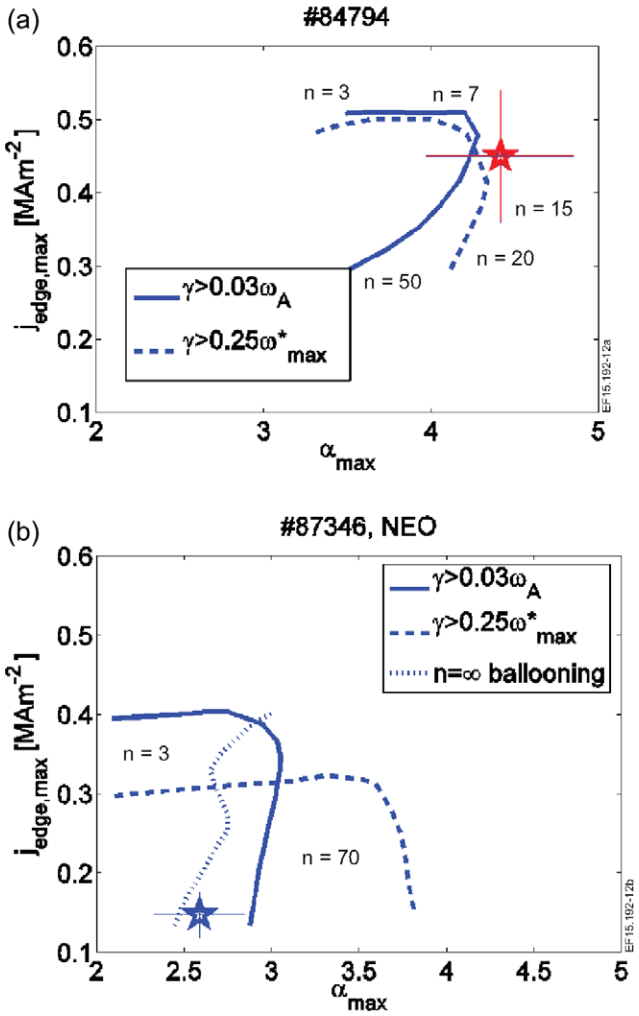

Figure 12. Effect of the choice of stability criterion for the P–B boundary on the pedestal stability analysis: (*a*) low gas/high power case (#84794, low collisionality), where the Sauter and NEO bootstrap current calculations are in very good agreement, but there is expansion of the ballooning boundary when $\gamma > 0.25\omega^*_{max}$ is used; (*b*) high gas/low power pedestal (#87346, high collisionality) with j_{BS} from NEO. The $n = \infty$ ballooning boundary is also indicated, for comparison.

representations. On the other hand, in the high collisionality case (#87346, figure 12(*b*)) the $\gamma > 0.25\omega^*_{max}$ criterion leads to a large expansion of the ballooning boundary and the operational point becomes deeply stable in this representation. For comparison, the stability boundary of the most unstable, $n = \infty$ ballooning mode is also shown (short dashed line).

4.2.3. Effect of maximum n number on the pedestal stability analysis. The edge stability analyses of figures 11 and 12 were performed extending the ELITE runs to a maximum toroidal mode number $n_{max} = 70$, which was needed to address the pedestal stability of the high collisionality shot #87346. We therefore investigate the effect of varying n_{max} in the ELITE calculations, which may be relevant to the edge stability analysis of cold pedestals close to the ballooning boundary. As an example, in figure 13 we compare for the high collisionality pedestal of shot #87346 and j_{BS} from

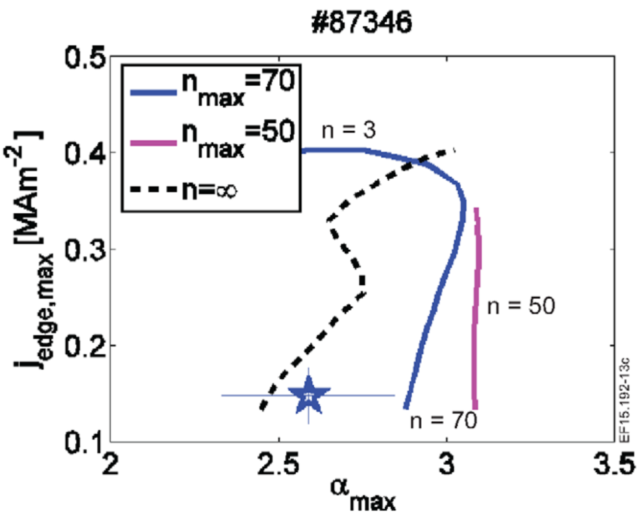

Figure 13. Sensitivity test of the choice of n_{max} in the ELITE calculations for the high gas/low power pedestal (#87346, high collisionality), with $\gamma > 0.03\ \omega_A$ stability criterion: $n_{max} = 70$ (blue) and $n_{max} = 50$ (magenta), with j_{BS} from NEO. The $n = \infty$ ballooning boundary is also indicated, for comparison (dashed line).

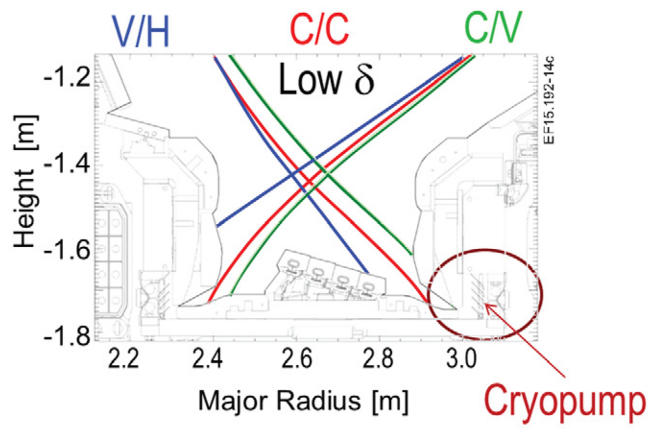

Figure 14. Divertor configurations used in the JET-ILW pedestal studies at low, average δ and constant main plasma shape, with MkII-HD divertor geometry: from left to right V/H (blue), C/C (red), C/V (green). The location of the divertor cryopump is also indicated.

NEO the simulations with ELITE run to $n = 50$ (pink boundaries) and $n = 70$ (blue boundaries). The stability criterion is $\gamma > 0.03\omega_A$. This sensitivity test indicates that increasing n from 50 and 70 in ELITE affects the ballooning boundary, as expected (see e.g. [28, 29]), and that the solution with $n = 70$ is closer to the experiment.

In summary, JET-ILW operation at high beta and low D_2 gas rates is a necessary condition for good pedestal (and core) performance. In these conditions the pedestals are largely consistent with the P–B paradigm and the EPED model can predict the pedestal height within the usually quoted ±20% confidence interval, as shown in ref [23]. In contrast, the weaker increase in pedestal pressure with power at high D_2 gas rates—necessary for W control, in particular at higher I_P/B_T—is not consistent with the peeling–ballooning model, even allowing for the large uncertainties associated with the stability analysis of cold pedestals close to the ballooning boundary discussed above. In these conditions, missing physics in the models—possibly linked with neutral penetration setting the pedestal width of both temperature and density—may be required to explain the onset of the ELM instability.

4.3. Variations in divertor configuration

The 2012 JET-ILW experiments showed that the energy confinement of low δ (~ 0.2), low beta ($\beta_N < 1.5$) ELMy H-modes is largely reduced due to the need for higher D_2 gas injection rates than in JET-C, as a measure against high W influxes through the pedestal into the core plasma [1]. These plasmas were run with a divertor configuration with the inner strike point on the **V**ertical target and the outer strike point on the bulk W, semi-**H**orizontal target (here denoted as V/H divertor configuration), as illustrated in figure 14.

New experiments in 2013–2014 aimed at optimizing the confinement of low δ, 2.5 MA/2.7 T ELMy H-modes have shown that when the effective neutral recycling is reduced, e.g. by placing both strike points close to the pumping duct (the so-called '**C**orner' divertor configuration, C/C, see figure 14), good confinement, H_{98} ~ 1 at β_N ~ 2, can be recovered in discharges that are steady over the entire additional heating phase (>10 × τ_E) [10]. Edge stability analysis with ELITE shows that in such cases the operational point is found at, or even marginally above, the P–B stability boundary.

The increase in total thermal stored energy, observed in the C/C configuration as compared to V/H, is related to an increase in core pressure at otherwise similar pedestal pressures. In particular, operation in C/C configuration, which leads to a 2–3 fold increase in sub-divertor neutral pressure and thus improved cryo-pumping compared to the V/H configuration, allows a decrease in $n_{e,PED}$ and an increase in $T_{e,PED}$ (and $T_{i,PED}$, as measured by edge charge exchange) at similar $p_{e,PED}$ values, while simultaneously maintaining W control and thus stable ELMy H-mode conditions. This is illustrated in the edge diagram—using ELM-averaged quantities—of figure 15(*a*) (red squares) for a dataset of low δ, 2.5 MA/2.4–2.7 T JET-ILW ELMy H-modes with auxiliary heating powers of 15–23 MW, provided by neutral beam injection. Conversely, in the V/H configuration (blue diamonds in figure 15(*a*)), with poorer pumping capability, similar pedestal pressures are achieved, but at lower $T_{e,PED}$ and higher $n_{e,PED}$ values, hence typically at higher edge collisionality (see figure 15(*b*)). The lower edge collisionality of ELMy H-modes in C/C configuration is well correlated with an increase in density peaking (figure 15(*b*)). This increase in density peaking with decreasing collisionality is consistent with the work of [30], which derives scalings for density peaking in tokamaks from a combined database of AUG and JET data, showing that collisionality is likely the most relevant parameter. More peaked core density profiles and thus higher pressure peaking, while T_e peaking remains unvaried, leads to an increase in global thermal stored energy in C/C configuration compared to V/H, at otherwise similar p_{PED} but lower collisionality, as shown by the electron kinetic profiles of figure 16 [31]. The best performing low δ, 2.5 MA/2.7 T ILW H-modes are those in C/C configuration achieving $T_{e,PED}$ values of 1–1.2 keV (see figure 15(*a*),

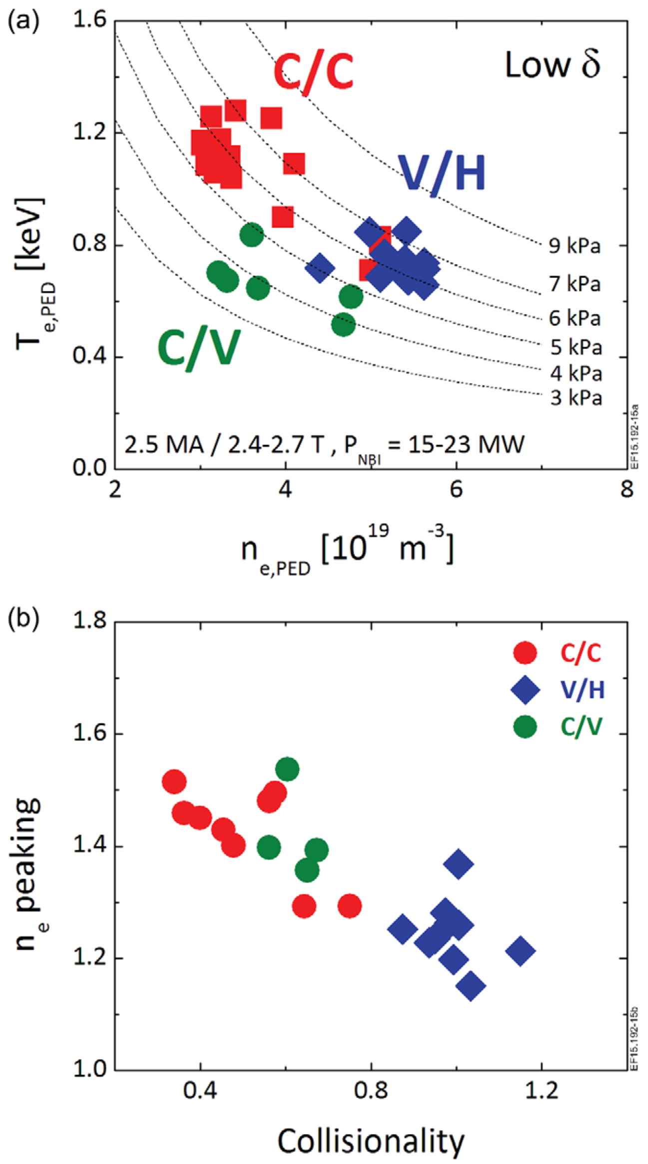

Figure 15. (*a*) $n_{\mathrm{e,PED}}$–$T_{\mathrm{e,PED}}$ diagram for the low δ ELMy H-mode experiments addressing the effect of varying divertor configuration on confinement: C/C (red squares), V/H (blue diamonds) and C/V (green circles) configurations at 2.5 MA/2.4–2.7 T and P_{NBI} = 15–23 MW; (*b*) density peaking factor versus average collisionality for the same discharges.

red squares and figure 1, open red circles), with H_{98} ~1 and β_{N} ~ 1.8–2.0 [32]. On the other hand, increasing the D_2 gas rate in C/C configuration eventually drives the discharges to conditions of low $T_{\mathrm{e,PED}}$ and higher $n_{\mathrm{e,PED}}$, similar to those in V/H configuration (red squares underneath blue diamonds in figure 15(*a*)), thus degrading the global energy confinement.

Experiments in 2013–14 have also investigated the effect of varying the inner and/or outer divertor strike point location on pedestal and global confinement. A deleterious effect on W_{PED} is observed in 2.5 MA/2.7 T H-modes, at similar input powers and D_2 gas rates as in V/H configuration, when the outer strike point is placed on the outer vertical divertor target and the inner strike point remains in the corner (denoted here C/V divertor configuration and illustrated in green in figure 14) while maintaining the main plasma shape constant [33]. In the C/V configuration, lower $n_{\mathrm{e,PED}}$ is observed than in V/H, but at similarly low $T_{\mathrm{e,PED}}$ values, as shown by the green circles in figure 15(*a*). This results in lower p_{PED} than in the V/H and C/C configurations. Good pumping is achieved in the C/V configuration, possibly also helped by the proximity of the inner strike point to the inner divertor corner participating in the effective pumping. This is likely to lead to the lower pedestal density observed in this configuration [33]. The average collisionality of the discharges in C/V configuration is intermediate between the higher ν^* in the V/H configuration and the lowest ν^* achieved in the C/C configuration and some increase in density peaking is observed from V/H to C/V (figures 15 and 16, top right panel). Thus, overall, the somewhat higher pressure peaking in C/V configuration, compared to V/H (figure 16), does not compensate for the large reduction in $p_{\mathrm{e,PED}}$. This leads to low pedestal *and* low core pressure in C/V configuration (figure 16) and thus to the lowest confinement of the three configurations investigated [33, 31].

Analysis of neutral re-circulation patterns in these experiments indicates that the neutral recycling in the divertor is not correlated with the observed variations in confinement, whereas the neutral pressure in the main chamber varies inversely with the energy confinement [33]. It is plausible that a change in divertor configuration may lead to a change in the leakage of neutrals towards the main chamber, thus affecting the main chamber neutral pressure. The pedestal pressure and the main chamber neutral pressure are found to be anti-correlated: the observed decrease in $T_{\mathrm{e,PED}}$ from C/C configuration to either V/H or C/V configurations appears to be correlated to an increase in main chamber neutral pressure (at fixed input power and D_2 injection rate) as analysed in further detail in [33]. However, it is not possible at present to establish a causal relationship between these observations. These findings are akin to the results of a recent analysis of the loss of confinement in high δ hybrid scenario in JET-C, showing a correlation between loss of confinement and increase in the neutral pressure and recycling in the main chamber [34, 15].

The changes in neutrals recirculation patterns induced when varying the divertor configuration are also correlated with differences in the ELM dynamics. For instance, when comparing ELMy H-modes in V/H versus C/C divertor configurations, it is observed that at higher $T_{\mathrm{e,PED}}$ (obtained in C/C configuration) the ELM energy losses, the width of the ELM affected volume and duration of the ELM crash are similar to those observed in JET-C [10]. Conversely, at lower $T_{\mathrm{e,PED}}$ values signatures of inter-ELM detachment are observed at the inner divertor, the MHD ELM crash time is longer in JET-ILW V/H configuration (~1–2 ms) [10, 3, 35] and the recovery of the density pedestal is delayed to 8–10 ms. This is possibly caused by a transient reduction in the D recycling coefficient after the ELM crash, with the W target plate acting as an additional particle sink, transiently during the ELM crash time, compared to the case with CFC divertor, where the large reservoir of fuel in co-deposits is likely to have compensated quasi instantaneously for the D outgassing [36].

2D divertor/SOL modelling of these discharges was carried out in order to investigate the interaction of the D neutrals with the pedestals. Charge exchange losses in the pedestal were found

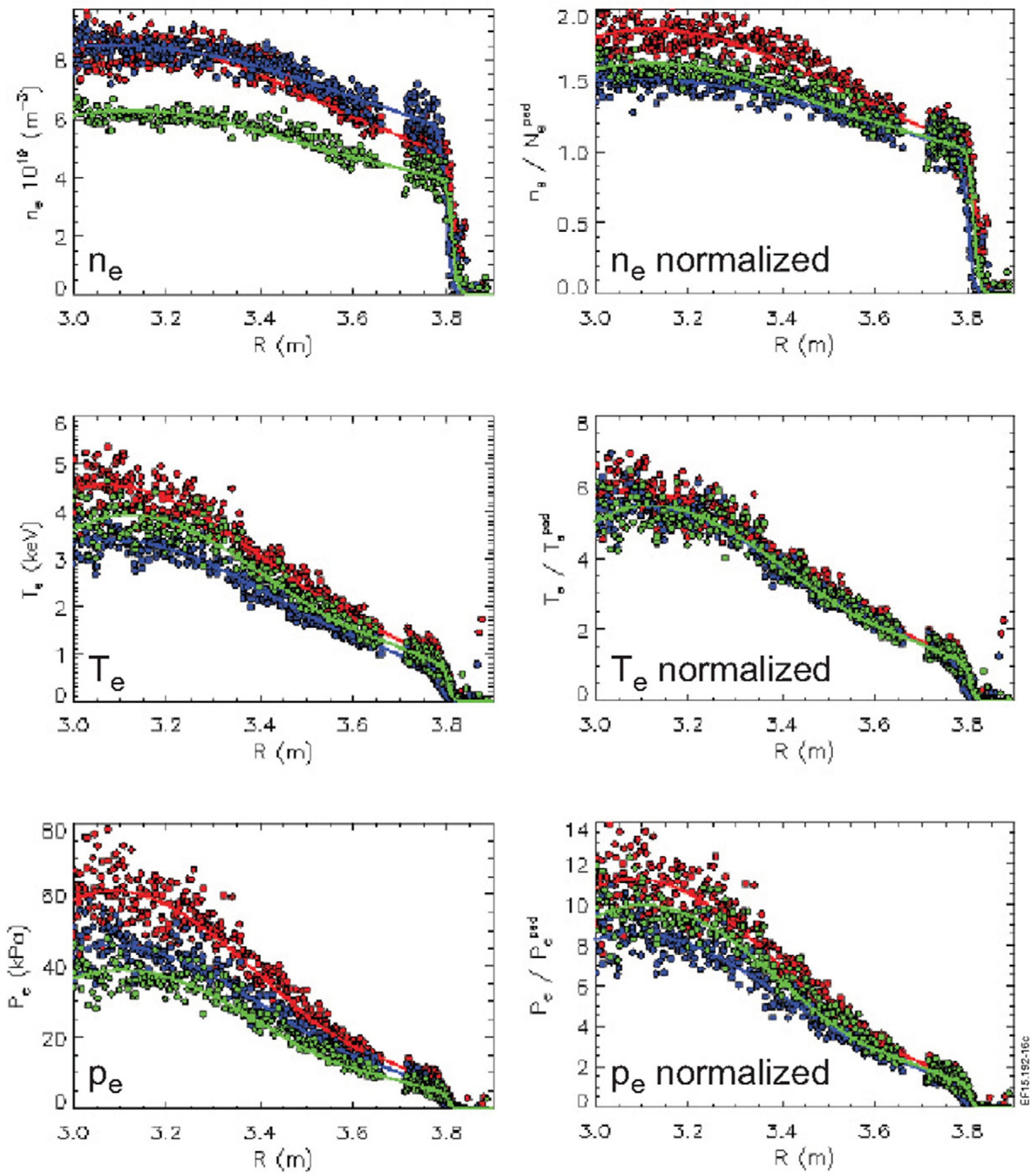

Figure 16. From top to bottom, ELM averaged radial profiles of electron density, temperature and pressure from HRTS (left panels) and corresponding profiles normalized to pedestal top values (right panels) for three selected discharges of figure 15, at same $P_{NBI} = 23$ MW and D_2 gas rate $= 2 \times 10^{22}$ e s^{-1}, and with different divertor configurations: C/C (red), V/H (blue) and C/V (green).

to be negligibly small and thus unlikely to explain the observed reduction in energy confinement [37, 38, 33]. Therefore, other possible mechanisms are under investigation and further experimental and modelling work is required in order to explain the physics underlying the degradation in confinement in JET-ILW with decreased pumping or increased D_2 gas injection.

4.4. Discussion

Because of the need to control W influxes into the plasma core, operation with some level of D_2 gas puffing is always necessary in JET-ILW to achieve stable ELMy H-mode conditions. Typically, increasing gas injection leads to a degradation of the pedestal energy confinement, while $n_{e,\,PED}$ remains largely unvaried, and overall to a reduction in normalized global confinement. Therefore, the lower pedestal performance of JET-ILW low beta, high density H-modes, compared to JET-C, is due in part to the need for higher gas puffing connected to W control. At high triangularity the degradation in pedestal performance is even more pronounced, as the lower $T_{e,PED}$ pushes the ILW pedestals close to the ballooning boundary, thus preventing improvement of the edge

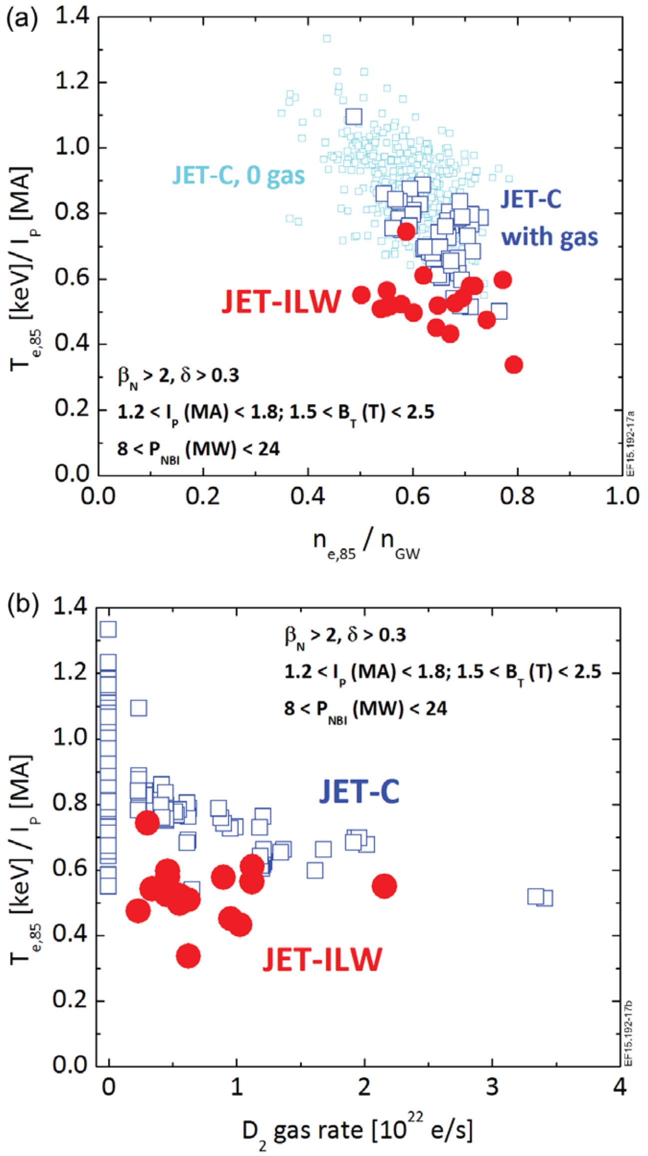

Figure 17. (*a*) Pedestal T_e and n_e diagram, with pressure normalized to I_P^2, as T_e/I_P and n_e/n_{GW} for JET-C and JET-ILW high beta ($\beta_N > 2$) H-modes at high triangularity ($\delta > 0.3$) at comparable operational parameters I_P, B_T, P_{NBI} and D_2 gas rate. T_e and n_e from HRTS at $\psi = 0.85$ are used as proxy for the ELM averaged $T_{e,PED}$ and $n_{e,PED}$; (*b*) for the same dataset, pedestal T_e versus D_2 gas rate.

stability due to plasma shaping, as discussed in section 2. The high beta JET-ILW ELMy H-modes, typically achieved with low gas injection and low main chamber neutral pressure, exhibit instead good normalized global confinement, comparable to JET-C, although they are not long term stable with respect to core W accumulation. In [3] it was reported from the 2011/12 experiments that also in such high beta H-modes the pedestal pressure is reduced in JET-ILW, but increased core profile peaking compensates for the reduction in pedestal confinement. This physics has been investigated by means of the beta scan experiments discussed in section 3 of this paper and in [15]. In particular, the stability of these pedestals has been shown to be consistent with the P–B paradigm both at low and high δ.

Extension of the JET H-mode database with the addition of the 2013/14 experiments allows us to confirm that in JET-ILW not only the H-modes at high gas injection but also those at lower gas rate and lower main chamber neutral pressure have reduced $T_{e,PED}$, and thus reduced pedestal performance, compared to JET-C. This is illustrated in figure 17 by extracting from the wider database JET-C and JET-ILW high beta H-modes ($\beta_N > 2$) at comparable input operational parameters. The selected high beta dataset is at high triangularity ($\delta > 0.3$), $1.2 < I_P$ (MA) < 1.8, $1.5 < B_T$ (T) < 2.5 and NBI input powers in the range $8 < P_{NBI}$ (MW) < 24 (without ICRH heating). Figure 17(*a*) shows the edge T_e–n_e diagram, with the pedestal pressure normalized to I_P^2 (since $\beta_{pol,PED} \sim p_{PED}/I_P^2$), therefore as T_e/I_P and n_e/n_{GW} (where n_{GW} is the Greenwald density). The ELM averaged electron temperature and density from HRTS, taken at $\psi = 0.85$, $T_{e,85}$ and $n_{e,85}$, are used here as proxy for the ELM averaged $T_{e,PED}$ and $n_{e,PED}$, respectively. The collinearity between $T_{e,85}$ and $n_{e,85}$ and $T_{e,PED}$ and $n_{e,PED}$ derived from *mtanh* fits of the HRTS profiles was verified for a selection of discharges of the database, confirming that $T_{e,85}$ and $n_{e,85}$ are indeed a good proxy for the T_e and n_e pedestal top values. It can be seen that the pedestal temperature is lower with ILW at all values of pedestal densities. Figure 17(*b*) shows the range of gas puff rates for the same discharges of figure 17(*a*): $T_{e,PED}$ is lower in JET-ILW at all values of D_2 gas puffing rate. The physics underlying this observation is not yet understood and is the subject of on-going study. Changes in wall recycling associated with the changes in wall composition from C to Be/W, in particular the dynamic phase associated with ELM crash and recovery (as discussed in section 4.3), may be responsible. As the degraded $T_{e,PED}$ can be recovered in the ILW with N_2 seeding to values approaching those of JET-C in some conditions (high δ, low beta H-modes at high D_2 gas rates), it could be that the strong reduction in C impurity concentration with the ILW is connected, in some way not yet understood, to the observed reduction in pedestal temperature.

Figure 17(*b*) also shows that the bulk of the JET-C high beta H-modes were run at 0 D_2 gas rate, a mode of operation which is no longer compatible with the W divertor. In addition, the JET-C high beta, high δ dataset shows a clear, monotonic decrease in $T_{e,PED}$ with increasing D_2 gas rate. This provides further evidence that the degradation of pedestal energy confinement with gas puffing is not purely a feature of the JET-ILW. The physics mechanism underlying the degradation of the pedestal temperature with increasing neutral content in the plasma is not understood to date. Because of its relevance to JET-ILW operation, and potentially to ITER's operation, it is currently the subject of intensive study.

5. Conclusions

H-mode experiments in JET with an ITER-like Be/W wall have challenged our current understanding of pedestal stability. On one hand the P–B paradigm describes well the JET-ILW pedestals at low gas injection (low neutral content in the plasma), both at low and high beta. On the other hand, high delta pedestals at high D_2 injection rates are not consistent with EPED model assumptions, as the pedestal widens at constant $\beta_{pol,PED}$ but with increasing $\nu^*_{e,PED}$ and thus the experiment deviates from the KBM-based dependence of the pedestal width with sqrt($\beta_{pol,PED}$) [23]. These results may indicate an additional dependence of the pedestal pressure width on other parameters, either directly or indirectly connected with the D neutral content in the plasma. The JET-ILW power scans at different D_2 gas injection rates (i.e. with varying neutral content in the plasma) indicate that the role of neutrals on pedestal stability should be addressed. Alternatively, it may be that the ELMs we observe in conditions of high neutral content, despite being of type I, are of resistive nature—e.g. more similar to type III ELMs—and therefore not described by the P–B paradigm. In these experiments the pedestal pressure width normalized to sqrt($\beta_{pol,PED}$) does not vary with $\nu^*_{e,PED}$ but is systematically wider at higher than at lower D_2 gas rates. This may imply that atomic physics effects could also contribute in setting the pedestal width. In some cases low beta, high δ plasmas are detached on the inner divertor leg and thus have a cold and dense X-point. This could affect the upstream kinetic profiles in the pedestal gradient region, thus the impact of changes in divertor/SOL conditions on pedestal stability should be investigated.

The reduction in energy confinement of JET-ILW low beta, high δ H-modes can be largely compensated by N_2 seeding: pedestal pressures approaching those of JET-C H-modes can be achieved at the same plasma density and auxiliary heating [2, 29]. The drastic reduction in C concentration from JET-C to JET-ILW and the beneficial effect of N_2 seeding on pedestal confinement point to the necessity of taking a closer look at the effect of low-*Z* impurities on pedestal stability. In particular, we need to understand what physics mechanisms lead, with N_2 seeding, to an increase in $T_{e,PED}$ in high δ plasmas in JET-ILW, while replacing C with Be is associated with a decrease in $T_{e,PED}$.

As it was found in local linear gyrokinetic calculations that most of the JET pedestal region is not limited by KBMs [39], we also need to think of how we can resolve the pedestal structure and its evolution. Global gyrokinetics and/or nonlinear GK should be considered as possible next steps in pedestal models. Alternatively, another paradigm may be needed, which does not invoke pedestal height limited by KBMs. Ultimately, future pedestal modelling should also address isotope effects, self-consistency between core and edge, effect of fast ions, difference in temperature and density profile structure, to name a few aspects that need to be considered in order to progress towards full predictive capability of the pedestal height. In view of ITER's requirements, in parallel with improved predictive capabilities, it may also be valuable to pursue with JET-ILW a pedestal solution involving small ELM size and low edge W impurity content.

Acknowledgments

This work has been carried out within the framework of the EUROfusion Consortium and has received funding from the EURATOM research and training programme 2014–2018 under grant agreement No 633053. The views and opinions expressed herein do not necessarily reflect those of the European Commission.

References

[1] Beurskens M. *et al* 2013 *Plasma Phys. Control. Fusion* **55** 124043
[2] Giroud C. *et al* 2013 *Nucl. Fusion* **53** 113025
[3] Beurskens M. *et al* 2014 *Nucl. Fusion* **54** 043001
[4] Saarelma S. *et al* 2014 *14th H-Mode Workshop (Fukuoka, Japan 2–4 October 2013)* http://tokusui.riam.kyushu-u.ac.jp/itmodeWS2013/link.html
[5] Wilson H.R. *et al* 2002 *Phys. Plasmas* **9** 1277
[6] Snyder P.B. *et al* 2002 *Phys. Plasmas* **9** 2037
[7] Snyder P. 2009 *Phys. Plasmas* **16** 056118
[8] Snyder P.B. *et al* 2011 *Nucl. Fusion* **51** 103016
[9] Snyder P.B. *et al* 2004 *Nucl. Fusion* **44** 320
[10] de la Luna E. *et al* 2014 Comparative study of high triangularity H-mode plasma performance in JET with Be/W and CFC wall [EX/P5-29] *Paper Presented at the 25th IAEA Int. Conf. on Fusion Energy (St Petersburg, Russia)*
[11] Saibene G. *et al* 2002 *Plasma Phys. Control. Fusion* **44** 1769
[12] Giroud C. *et al* 2012 *Nucl. Fusion* **52** 063022
[13] Leyland M. *et al* 2013 *Nucl. Fusion* **53** 083028
[14] Maggi C.F. *et al* 2014 *Nucl. Fusion* **54** 023007
[15] Challis C.D. *et al* 2015 *Nucl. Fusion* **55** 053031
[16] Groebner R.G. *et al* 1998 *Phys. Plasmas* **5** 1800
[17] Frassinetti L. *et al* 2012 *Rev. Sci. Instrum.* **83** 013506
[18] Sauter O. *et al* 1999 *Phys. Plasmas* **6** 2835
[19] Sauter O. *et al* 2002 *Phys. Plasmas* **9** 5140 (erratum)
[20] Saarelma S. *et al* 2015 The effects of impurities and core pressure on pedestal stability in the Joint European Torus (JET) *Phys. Plasmas* **22** 056115
[21] Neu R. *et al* 2013 *Phys. Plasmas* **20** 056111
[22] Zohm H. *et al* 1996 *Plasma Phys. Control. Fusion* **38** 105
[23] Leyland M. *et al* 2015 *Nucl. Fusion* **55** 013019
[24] Saarelma S. *et al* 2009 *Plasma Phys. Control. Fusion* **51** 035001
[25] Belli E. and Candy J. 2008 *Plasma Phys. Control. Fusion* **50** 095010
[26] Belli E. and Candy J. 2012 *Plasma Phys. Control. Fusion* **54** 015015
[27] Belli E.A. *et al* 2014 *Plasma Phys. Control. Fusion* **56** 045006
[28] Maget P. *et al* 2013 *Nucl. Fusion* **53** 093011
[29] Giroud C. *et al* 2015 *Plasma Phys. Control. Fusion* **57** 035004
[30] Angioni C. *et al* 2007 *Nucl Fusion* **47** 1326
[31] Frassinetti L. *et al* 2014 Effect of the divertor geometry on pedestal confinement in JET-ILW *41st EPS Conf. on Plasma Physics (Berlin, Germany)* P1-030
[32] Nunes I. *et al* 2014 Compatibility of high performance operation with JET-ILW [EX/9-2] *Paper Presented at the 25th IAEA Int. Conf. on Fusion Energy (St. Petersburg, Russia) (13–18 October 2014)*
[33] Joffrin E. *et al* 2014 Impact of divertor geometry on ITER scenarios performance in the JET metallic wall [EX/P5-4] *Paper Presented at the 25th IAEA Int. Conf. on Fusion Energy (St Petersburg, Russia) (13–18 October 2014)*
[34] Joffrin E. *et al* 2014 *41st EPS Conf. on Plasma Physics (Berlin, Germany)* O4.125
[35] Frassinetti L. *et al* 2015 *Nucl Fusion* **55** 023007
[36] Brezinsek S. *et al* 2015 *J. Nucl. Mater.* **463** 11–21
[37] Tamain P. *et al* 2014 *J. Nucl. Mater.* **463** 450–4
[38] Jarvinen A. *et al* 2014 Comparison of H-mode plasmas in JET-ILW and JET-C with and without nitrogen seeding [TH/P5-34] *Paper Presented at the 25th IAEA Int. Conf. on Fusion Energy (St Petersburg, Russian Federation)*
[39] Saarelma S. *et al* 2013 *Nucl. Fusion* **53** 123012
[40] Romanelli F. *et al* 2014 *Paper Presented at the 25th IAEA Int. Conf on Fusion energy (St Petersburg, Russian 13–18 October 2014)*